

Chapter 2

Fiber Fuse Propagation Modes

Nothing is more revealing than movement.

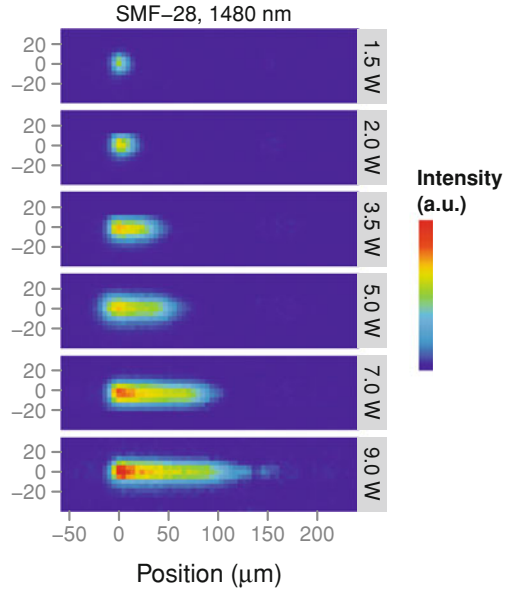
—Martha Graham

2.1 Introduction

In spite of the 25-year history of fiber fuse research, most researchers still see a fiber fuse as a moving point without an internal structure as summarized in the previous chapter. This is partly because the time for observing this moving object within the scope of their measuring devices is very short. To deepen our knowledge of the fiber fuse, more precise and extensive measurements are needed. In the following three chapters, I try to clarify the inner structure and action of a fiber fuse generated in standard single-mode fibers by focusing on its motion (this chapter), periodic void formation (Chap. 3) and its pump power modulation and response (Chap. 4).

Although the fusing speed is known to increase monotonously with pump power as summarized in Sect. 1.3, the generated damage exhibits various patterns as shown in Fig. 1.8. Thus, the pump power dependence of the following three characteristics is precisely investigated; an in situ image of fiber fuse propagation, void shape, and propagation speed. As a result, it was found that the fusing speed near the propagation threshold deviates from an extrapolated line based on the higher pump power side due to the shrinkage of the confined plasma. This chapter describes the details of the fiber fuse propagation behavior and classifies it into three modes; unstable, unimodal, and cylindrical.

Fig. 2.1 In situ images of fiber fuse propagation captured with an ultrahigh-speed video camera. Original *gray-scale* images are converted to *color-scale* images. See Box 2.1 (b) for details



2.2 In Situ Observation of Fiber Fuse Propagation

An orthodox approach to investigate a moving object involves taking a high-speed photograph. Since a fiber fuse moves at roughly 1 m/s, the time for capturing it within the scope of the camera, for a distance of 1 mm for example, is less than 1 ms. Moreover, the exposure time should be as small as possible to avoid overexposure to the strong light emission from the plasma. After preliminary trials in 2004 [1, 2, 4] (see also Box 2.1 (a)), the pump power dependence of the light emission profile was revealed as shown in Fig. 2.1 (see also Box 2.1 (b)), which is a reproduction based on the original data [5].

The fibers used are a commercially produced standard single-mode fiber, SMF-28e (Corning). The light source was a Raman fiber laser (CW, wavelength: 1.48 μm). A fiber fuse was initiated by the local heating of a fiber delivering several watts of light (see Fig. 2.2 (1)). Then, the pump power was reduced to a certain value (2), and the laser oscillation was stopped after the picture taking was completed (3). All the laser operations were performed via a personal computer.

Box 2.1 Videos providing microscopic view of fiber fuse propagation and void formation.

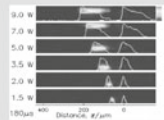
(a) First trial in situ observation in August 2004.



<http://imeji.nims.go.jp/collection/8/item/9>
Duration: 0:03
Fiber: SMF-28 (Corning)
Pump laser: 1480 nm, 9W
Camera: FASTCAM-MAX (Photron)
Speed: 100,000 fps Exposure time: 1 μ s
References: Fig. 4 in [4]



(b) Pump power dependence of fiber fuse propagation behavior. Original gray-scale images are converted to color-scale images.



<http://imeji.nims.go.jp/collection/8/item/11>
Duration: 0:18
Fiber: SMF-28 (Corning)
Pump laser: 1480 nm
Camera: FASTCAM-APX RS (Photron)
Speed: 250,000 fps Exposure time: 1 μ s
References: Fig. 2.1, Fig. 3 in [5]



(c) Fiber fuse propagation and void formation.



<http://imeji.nims.go.jp/collection/8/item/10>
Duration: 0:09
Fiber: SMF-28e (Corning)
immersed in index matching oil
Pump laser: 1480 nm
Camera: FASTCAM SA5 (Photron)
Speed: 30,000 fps Exposure time: 33.3 μ s
References: Fig. 4.8

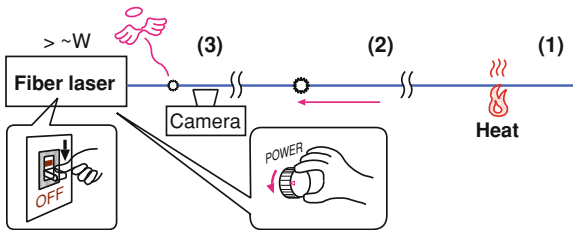
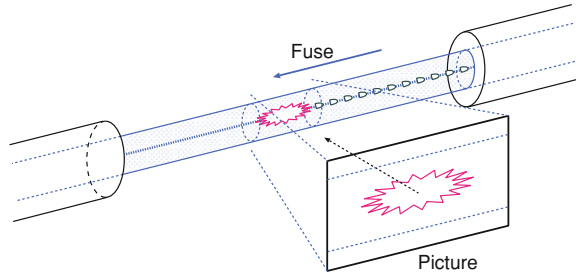


Fig. 2.2 Experimental setup for taking pictures of fiber fuse propagation

Figure 2.3 shows the configuration for taking fiber fuse pictures. The acrylate coating was removed from a segment including the field of vision. The confined plasma propagated from right to left. This is true for all the figures in this book. Since the fiber acts as a cylindrical lens, we should note that the image near the core region is non-linearly expanded in the vertical direction.

Fig. 2.3 Geometrical arrangement of a test fiber and its photograph



The most important finding from Fig. 2.1 is that there are two types of emission profile along the fiber axis; a symmetric unimodal profile, pumped at 2 W or less, and an asymmetric profile. Their propagation speeds were calculated from successive video images and showed a roughly linear dependence on pump power [5].

2.3 Void Track Variation with Pump Power

Given the difficulty involved in investigating a moving object, the next best subject for investigation is the damage sites that it leaves. The first void of the damage train is the place where confined plasma disappeared due to pump exhaustion. The first void shape variation with pump power was reported in 2005 [5], and Fig. 2.4 reproduces that result with better image quality and enhanced pump power precision. The value before the shutdown was determined with a precision of 0.01 W on the basis of the power stabilization behavior of the light source observed in preliminary experiments. The damage sites in the core region were observed with a digital optical microscope where the samples were immersed in index matching oil.

The volume of the first void increases with the pump power, and its shape changes at about 2 W from a spheroid to a long partially cylindrical void. This tendency agrees well with the in situ observation result shown in Fig. 2.1. These void shapes are expected to retain the outline of the confined plasma if the quenching rate of the glass melt is not delayed by some external conditions including the pump power decay rate. Thus, the decay time of the plasma light emission after the pump laser shutdown was estimated on the basis of ultrahigh-speed photography (see Fig. 2.5). It is no more than $7 \mu\text{s}$ [3], which is far shorter than the time needed for heat diffusion from the core to the cladding surface, that is, a few milliseconds (see Fig. 1.3). Thus, it is reasonable to assume that the plasma outline is frozen into the void shape.

Then, it is possible to classify these plasma shapes into the following three types on the basis of Fig. 2.4 and the void diameter plotted in Fig. 2.6b, c.

1. a spheroid whose diameter increases with the pump power (see Fig. 2.4a and b; \times in Fig. 2.6)
2. a spheroid with a constant diameter ((c) and (d); \bigcirc)
3. a long partially cylindrical void with a constant diameter ((e)–(h); \square).

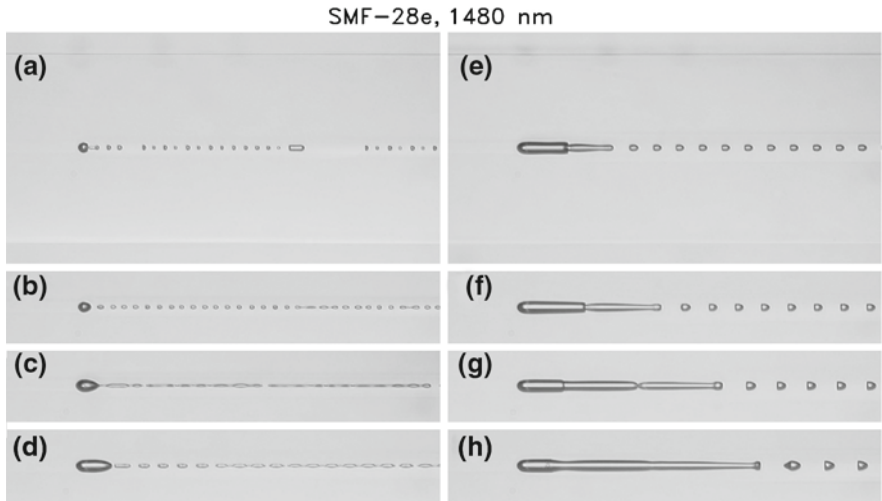
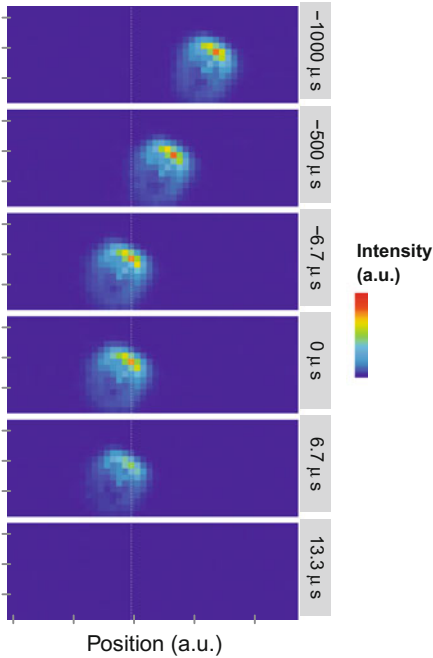


Fig. 2.4 Optical micrographs showing the front part of the fiber fuse damage generated in single-mode silica glass fibers (SMF-28e). The pump laser powers are **a** 1.33 W (propagation threshold), **b** 1.36 W, **c** 1.47 W, **d** 2.03 W, **e** 3.42 W, **f** 5.00 W, **g** 6.99 W, and **h** 8.99 W; wavelength: 1,480 nm. The two thin lines at the *top* and *bottom* of **a** and **e** are the edges of the fiber, whose diameter is 125 μm

Fig. 2.5 In situ images capturing the moment of fiber fuse termination caused by a manual shutdown of the pump laser at $t = 0$ ms. The exposure time was 3.9 μs . The emission had disappeared completely by the second frame after the shutdown. The *donut shape* of the image is because it is out of focus



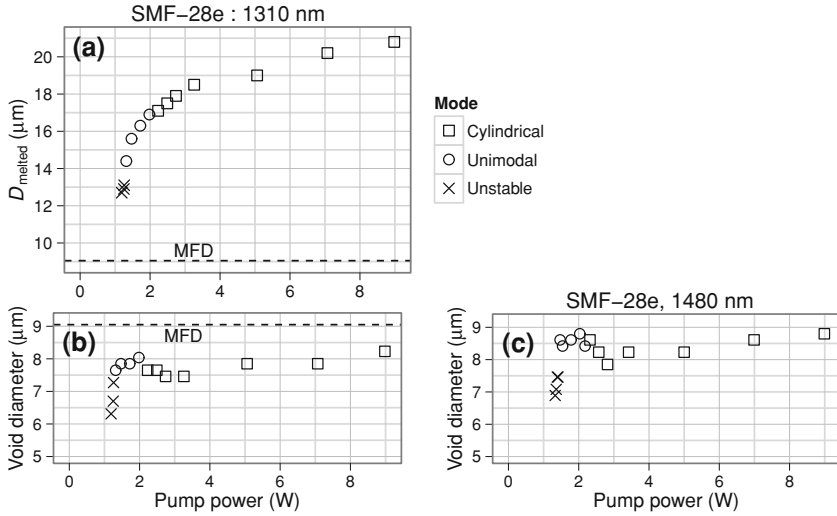


Fig. 2.6 a Pump power dependence of the diameter of the modified area in the refractive index and b and c the first void diameter that remain after the passage of a fiber fuse in SMF-28e. The wavelength is 1,310 nm for (a) and (b), and 1,480 nm for (c)

For explanatory convenience, they are referred to as unstable, unimodal, and cylindrical modes, respectively.

This void diameter saturation in unimodal and cylindrical modes is due to the confined distribution of the pump power at the fiber core. The ceiling value is less than the MFD as shown in Fig. 2.6b. Thus, the plasma length along the fiber increases with the pump power as shown in Figs. 2.1 and 2.4.

At the same time, the plasma temperature is expected to increase. This trend is extracted from the damaged fibers as a cylindrical area surrounding the damage whose refractive index is modified due to the propagation of hot plasma. The outline of this area is seen clearly under tilted illumination as shown in Fig. 1.8. The diameter of this area, D_{melted} , increases monotonously with the pump power as shown in Fig. 2.6a.

The photographs in Fig. 2.4 also show a variation in the void train left after the first void. Periodicity appears in the cylindrical mode (e–h) and in a limited pump power range in the unstable mode (b), whereas it is broken in the unimodal and unstable modes (a, c, d). This will be discussed in detail in the next chapter.

2.4 Precise Measurement of Propagation Speed

The above three-way classification of plasma shape raises the question of whether the fuse propagation speed really increases linearly with the pump power. In fact, a recent high-precision velocity measurement revealed a linearity deviation on the

Fig. 2.7 Pump power dependence of fiber fuse propagation speed in two types of single-mode fibers

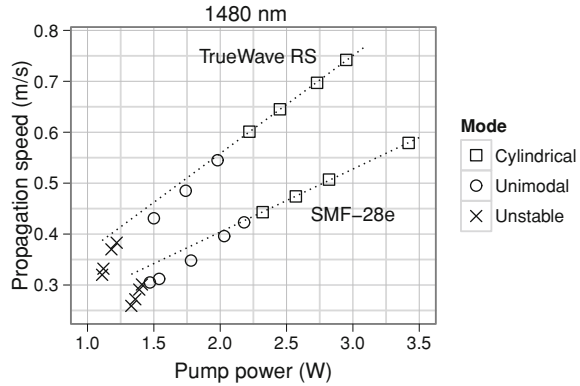
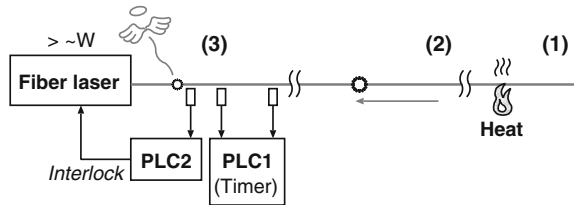


Fig. 2.8 Experimental setup for propagation speed measurement. *PLC* programmable logic controller



low-energy side as shown in Fig. 2.7 [6, 7]. The propagation speed was calculated from the time difference between two photosensors placed along a fiber 80 mm apart (see Fig. 2.8 (3)). The time unit is 0.1 ms, and the error in the calculated velocities is estimated to be about ± 0.01 m/s.

Figure 2.7 shows the results for two types of fibers, SMF-28e and TrueWave RS (OFS), with different MFDs, 10.4 ± 0.5 and 8.4 ± 0.6 (product specifications at 1,550 nm), respectively. The velocity of TrueWave RS is larger than that of SMF-28e owing to its smaller MFD. However, both show similar pump power dependence. In addition, their propagation threshold power values varies in proportion to MFD [7] (see also Sect. 1.4).

Each dotted line is the result of a least squares fit to the four open squares on the right and shows that the remaining points deviate from the line. The deviation becomes larger near the propagation threshold. The slope becomes about three times larger than that shown as a dotted line when the pump power is less than 1.4 W. This behavior is coupled with the void diameter saturation described in the previous section. The cross section of confined plasma perpendicular to the pump beam stops increasing with the pump power at a certain threshold value near 1.4 W. Another slight slope change found at around 2.2 W is due to the geometrical change of the confined plasma from a spheroid to a long partially cylindrical void.

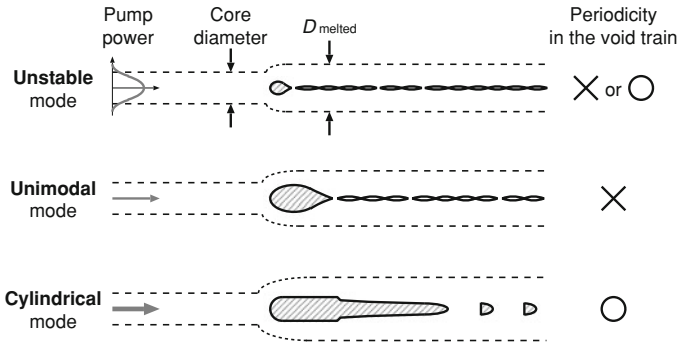


Fig. 2.9 Fiber fuse propagation modes based on the shape and volume of the confined plasma

2.5 Summary

Three types of propagation modes are revealed on the basis of in situ observation and speed measurement of fiber fuse propagation and the damage morphology of fused fibers. The difference comes from the plasma volume confined in the fiber core as summarized in Fig. 2.9.

References

1. I.A. Bufetov, E.M. Dianov, Optical discharge in optical fibers. *Phys. Usp.* **48**(1), 91–94 (2005). doi:[10.1070/PU2005v048n01ABEH002081](https://doi.org/10.1070/PU2005v048n01ABEH002081)
2. S. Todoroki, In-situ Observation of Fiber-Fuse Propagation, in *Proceedings of the 30th European Conference Optical Communication Post-deadline papers*, pp. 32–33. Kista Photonics Research Center, Stockholm, Sweden, 2004 (Th 4.3.3)
3. S. Todoroki, Animation of fiber fuse damage, demonstrating periodic void formation. *Opt. Lett.* **30**(19), 2551–2553 (2005). doi:[10.1364/OL.30.002551](https://doi.org/10.1364/OL.30.002551)
4. S. Todoroki, In-situ observation of fiber-fuse propagation. *Jpn. J. Appl. Phys.* **44**(6A), 4022–4024 (2005). doi:[10.1143/JJAP.44.4022](https://doi.org/10.1143/JJAP.44.4022)
5. S. Todoroki, Origin of periodic void formation during fiber fuse. *Opt. Express* **13**(17), 6381–6389 (2005). doi:[10.1364/OPEX.13.006381](https://doi.org/10.1364/OPEX.13.006381)
6. S. Todoroki, Fiber Fuse Propagation Modes in Typical Single-Mode Fibers, in *Optical Fiber Communication Conference, OSA Technical Digest* (Optical Society of America, USA, 2013). doi:[10.1364/NFOEC.2013.JW2A.11](https://doi.org/10.1364/NFOEC.2013.JW2A.11). Paper JW2A.11
7. S. Todoroki, Modes and threshold power of fiber fuse propagation. *IEICE Trans. Commun. B* **J96-B**(3), 243–248 (2013) (in Japanese)

Fiber Fuse

Light-Induced Continuous Breakdown of Silica Glass
Optical Fiber

Todoroki, S.-i.

2014, XIII, 58 p. 51 illus., 16 illus. in color., Softcover

ISBN: 978-4-431-54576-7